JOURNAL OF THERMOPHYSICS AND HEAT TRANSFER
Vol. 16, No. 4, October–December 2002

Thermal Analysis of the ALR8(SI) Plutonium Storage Container

D. L. James* and S. Stevkovski†
Texas Tech University, Lubbock, Texas 79409-1021

As a result of the end of the cold war, at least 11,000, and possibly up to 20,000, plutonium pits are projected to be stored in temporary storage facilities in the United States for up to 50 years. The storage container, the ALR8(SI), must be investigated for quality and longevity requirements. As a part of validating the U.S. Department of Energy's quality requirements, a computer model was developed and validated to predict the temperature distribution within both the stored components and the internal structure of the ALR8(SI) container to analyze the thermal performance of the container. Experimental data were obtained and served as a comparison for examining the validity of the numerical model. The thermal response of the ALR8(SI) under normal storage conditions was investigated experimentally. Results were obtained for different values of heat generation rate (15, 20, 25, and 30 W), outside container temperature (20, 25, and 30°C), and different backfill gases (air, argon, and helium). A finite element model consisting of a thermal and a flow domain was created and solved simultaneously using SDRC I-DEAS Master Series 6. Solutions were obtained for most of the experiments performed. The predicted temperature distribution matched quite well in magnitude with the experimental data. For most locations, predicted temperatures deviated less than 2°C from the experimental temperatures, whereas the maximum deviation was around 4°C. In most cases, the maximum-recorded temperature exceeded the quality limit of 60°C. A theoretical study of the heat transfer mechanisms showed either conduction through the backfill gas or natural convection as the primary mode of heat transfer, depending on the backfill gas. In an attempt to reduce the interior temperatures of the ALR8(SI), a modification to one of the ALR8(SI) components was made in the numerical model to enhance heat transfer. Solutions of this modified container predicted significantly lower temperatures of the interior.

Nomenclature

A	=	surface area, m^2
a	=	scale factors
C	=	contact resistance factor
D_o; D_i	=	outside; inside diameter, m
F_{ij}	=	view factor
Gr	=	Grashof number
g	=	gravity, m/s^2
h	=	convective heat transfer coefficient, W/m^2K
k	=	thermal conductivity, W/m K
L	=	effective gap thickness, m
P	=	pressure, N/m^2
Pr	=	Prandtl number
q'	=	heat flux per unit length, W/m
q'''_{gen}	=	heat generation per unit volume, W/m^3
Ra	=	Rayleigh number
T	=	temperature, K
u_i	=	orthogonal curvilinear coordinates
V	=	velocity, m/s
α	=	thermal diffusion coefficient, m^2/s
β	=	expansion coefficient, 1/K
δ	=	effective gap for thermal couplings, m
ν	=	kinematic viscosity, m^2/s
ρ	=	density, kg/m^3
σ	=	Stefan–Boltzmann constant, 5.67×10^{-8} $W/(m^2K^4)$

Subscripts

a	=	advective
eff	=	effective
i	=	ith component or direction
r	=	radiative
∞	=	ambient

Received 24 April 2000; revision received 3 May 2002; accepted for publication 24 May 2002.

*Associate Professor, Department of Mechanical Engineering.
†Graduate Student, Department of Mechanical Engineering.

Introduction

As a result of the end of the cold war, at least 11,000, and possibly up to 20,000, plutonium pits are projected to be stored in temporary storage facilities in the United States for up to 50 years. The storage container, the ALR8(SI), must be investigated for quality and longevity requirements. As a part of validating the U.S. Department of Energy's quality requirements, a computer model was developed and validated to predict the temperature distribution within both the stored components and the internal structure of the ALR8(SI) container to analyze the thermal performance of the container. One part of the quality requirements is to limit the maximum temperature within the storage container to less than 60°C. This research was specifically initiated to perform a detailed thermal analysis of the ALR8(SI) container to understand the mechanisms by which heat is transferred out of the container and to provide thermal design changes to the container to meet this one quality requirement.

Several studies for the design of interim and permanent storage containers specific to the evaluation of mechanical performance for a given container have been performed. A session entitled "Transportation, Storage, and Disposal of Radioactive Materials" was a part of the 1997 American Society of Mechanical Engineers Pressure Vessels and Piping Conference. As a part of the mechanical design, simplified thermal analyses have been included in some of the work presented at the aforementioned conference. A more detailed thermal modeling of metal ingots stored in food pack cans (two-can and three-can systems) was included at that conference.[1] The cans were placed concentrically within another and were oriented vertically. The thermal code used did not include a flow solver. A computational fluid dynamics code was used to calculate an effective conductivity for the natural convection that was used in the thermal code. It was concluded that including natural convection in the complete thermal analysis lowered the ingot temperature and that radiative heat transfer between the inner and outer can was insignificant.

A one-dimensional transient thermal analysis of a shipping container that was subjected to diurnal-like variations in solar insolation

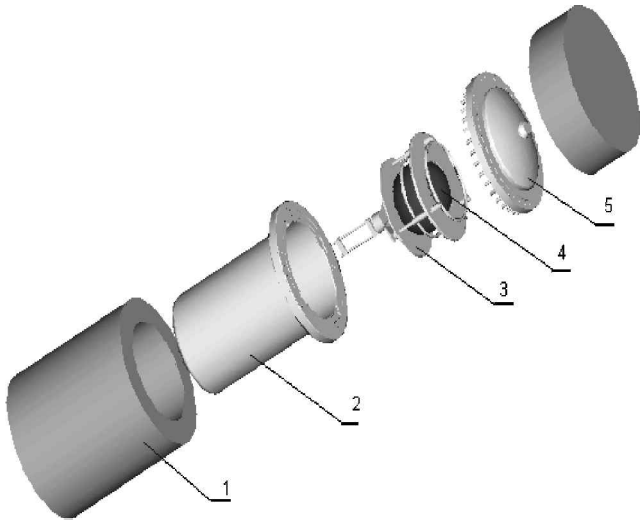

Fig. 1 Exploded view of the ALR8(SI) storage container components.

(400 W/m^2 for 12 h on, then off) was conducted at the Oak Ridge Y-12 Plant.[2] The container was modeled as two horizontal, concentric, infinitely long cylinders. Between the inner and outer cylinder existed two concentric rings of Celotex™. A 6.35-mm (0.25-in.) gap existed between each ring. Heat transfer between the gap was assumed to occur solely by radiation. An unknown inert gas filled the inner container. The quasi-steady-state solution over a 24-h period predicted only a 1°C variation in the inner container temperature when the outer container temperature varied by 45°C.

The ALR8(SI) storage container is significantly different from the containers modeled by previous investigators.[1,2] The ALR8(SI) is a modification of the ALR8 shipping container, a 0.114-m^3 (30-gal) mild-steel drum with an internal fixture for supporting the pit. The new container includes a hermetically sealed stainless-steel insert, and its components are shown in Fig. 1. The plutonium pit (4; Fig. 1) is placed in an internal supporting fixture that is referred to as the birdcage (3; Fig. 1). The birdcage is placed within the sealed stainless steel insert (2; Fig. 1). The upper disk of the birdcage sits on the flange of the sealed insert and is gripped between the sealed insert body and its cover (5; Fig. 1). Celotex packaging material (1; Fig. 1) fills the volume between the sealed insert and a 2030 drum (740 × 500 mm) that is not shown.

An ALR8(SI) container was provided by the Amarillo National Resources Center. For experimental purposes, a component was made to model the thermal generation of the plutonium. It was a hollow, bowling-ball-sized stainless-steel sphere. Joulian heating was used to simulate the thermal energy generation caused by the radioactive decay of the plutonium. By the passage of an electric current through a resistor placed in the center of the sphere, a uniform radiative heat flux was imposed on the inner surface of the pit simulator.

Creating a numerical model from the ALR8(SI) was a relatively complex problem. All three modes of heat transfer mechanisms are important in a detailed thermal analysis of the ALR8(SI) container. In steady-state storage conditions, the same amount of heat that is generated in the plutonium pit was transferred to the ambient from the exterior ALR8(SI) surfaces. The local heat transfer coefficient on the exterior surfaces of the 2030 drum depended on the temperature distribution of the ALR8(SI), as well as on the ambient temperature and conditions. Because these conditions were not known a priori, a constant boundary temperature was applied, thus reducing the complexity of the external boundary condition for the numerical modeling while providing an effective comparison of the experimental and numerical results. Previous research[2] has demonstrated that external boundary conditions have little effect on the internal temperature distribution under normal conditions and, hence, on the heat transfer mechanisms within the container.

The thermal analysis of the ALR8(SI) consisted of both solid components and a gaseous medium; therefore, two domains were created for the numerical model. One domain consisted of the solid components, and the other was the fluid domain that was occupied by the backfill gas in the void space within the sealed insert. The governing equations were different for both domains. In the solid domain, the governing equation for steady-state heat conduction in general orthogonal curvilinear coordinates was given by[3]

$$\frac{1}{a}\left[\frac{\partial}{\partial u_1}\left(k_i\frac{a}{a_1^2}\frac{\partial T}{\partial u_1}\right)+\frac{\partial}{\partial u_2}\left(k_i\frac{a}{a_2^2}\frac{\partial T}{\partial u_2}\right)+\frac{\partial}{\partial u_3}\left(k_i\frac{a}{a_3^2}\frac{\partial T}{\partial u_3}\right)\right]+q'''_{\text{gen}}=0 \tag{1}$$

where $a=a_1a_2a_3$ are functions of the coordinates and were known once the functional relationship between the rectangular and orthogonal curvilinear system was specified. The governing equation must be written for each material within the ALR8(SI) container. Continuity of temperature and heat flux between any two adjacent solid materials cannot be assumed because there are gaps that allow heat to be transferred in a direction that is not normal to the solid surfaces that cannot be neglected between the components of the ALR8(SI). In certain cases, there was no contact between two adjacent materials, but a relatively large void space separated them. These unavoidable thermal contact resistances complicated the problem furthermore.

In the fluid flow domain, the behavior of the backfill gas is governed by the mass, momentum, and energy conservation equations. In case of natural convection for which the Boussinesq approximation is valid,[4] they are given by

$$\bar{\nabla}\cdot\bar{V}=0 \tag{2}$$

$$\frac{\mathrm{D}\bar{V}}{\mathrm{D}t}=-\frac{1}{\rho}\nabla P+\nu\nabla^2\bar{V}+\bar{g}\beta(T-T_\infty) \tag{3}$$

$$\frac{\mathrm{D}T}{\mathrm{D}t}=\alpha\nabla^2T \tag{4}$$

The gravity force in this case acts in the negative z direction. The expansion coefficient β, for an ideal gas, is given by[4]

$$\beta=1/T \tag{5}$$

The solution of Eqs. (2–4) was coupled with the solution of the conduction-domain problem, Eq. (1). Therefore, to predict the temperature distribution in the ALR8(SI) container, the conduction analysis was coupled to the fluid flow analysis with the added complication of radiative heat transfer.

A solver that was capable of solving the coupled fluid–conduction problem with surface radiation and that had the ability to include contact resistances needed to predict the temperature distribution within the ALR8(SI) was the SDRC I-DEAS electronics system cooling (ESC) (Ref. 5) solver. This solver, mainly used for ESC problems, can solve coupled thermal/flow problems. In this work, SDRC I-DEAS was used for creating finite element models of the ALR8(SI) container and for the numerical simulation data presented.

Experimental Apparatus

The experimental setup will be explained with the aid of Figs. 1 and 2. The plutonium pit simulator (4; Fig. 1) was manufactured from stainless-steel 316, and it consisted of two hemispheres, each with a diameter of 215 mm and wall thickness of 15 mm. The hemispheres were aligned to fit together when inserted into the birdcage (3; Fig. 1), thus creating the bowling-ball-sized sphere. To simulate heat generation caused by the plutonium decay, a 5-Ω wirewound porcelain cylindrical resistor was positioned in the center of the sphere using a plexiglass rod. Because the rod has a very low thermal conductivity, the heat generated in the resistor was mainly radiated to the inner surface of the pit simulator. The resistor was connected to a dc power supply via electric wires passing through a small gap between the two hemispheres. Varying the

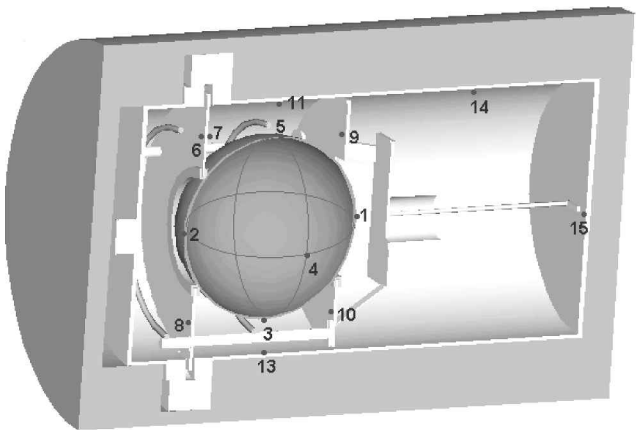

Fig. 2 Sectional view of the sealed insert, showing the interior thermocouple locations.

dc voltage applied to the resistor controlled the heat generation. The uncertainty in the heat generation was calculated to be ±2% (Ref. 6). To achieve a connection with the resistor from outside of the sealed insert without losing its hermetic properties, a multiconductive feedthrough was used. The feedthrough allowed up to 16 probes to be inserted within the sealed insert (see Fig. 2 for the interior thermocouple locations) through the 1.6-mm ($\frac{1}{16}$-in.) openings. The feedthrough passages were sealed with conical ferrules. Thermocouples were placed at different positions and connected to the data acquisition system. A computer using a virtual instrument program file created in LabVIEW™ converted the electromagnetic force generated at the junctions into temperature values. Tygon tubing was wrapped around the exterior of the ALR8(SI) container. A constant temperature fluid was circulated around the exterior of the ALR8(SI) to provide an isothermal boundary condition to within ±0.2°C (Ref. 6). Having an isothermal boundary condition provided an "exact" comparison of the experimental and numerical results and provided more physical insight into the mechanisms for heat transfer within the container.

Experimental Procedure

After the thermocouples were attached to the corresponding locations, the components of the ALR8(SI) were carefully assembled. The storage container was positioned horizontally, referred to as the stage-right configuration, as illustrated in Fig. 2. The experimental ALR8(SI) was placed on a wooden structure to avoid undesirable heat transfer from/to the container. The air was then evacuated from the sealed insert to a vacuum pressure of 670 mmHg (89 kPa), and it was filled with argon, helium, or dry air to ambient pressure. The temperature of the coolant and the dc voltage were adjusted corresponding to the desired outside boundary condition and pit power generation for the ongoing series. A steady-state condition was reached after 24–48 h when initial conditions were at ambient and after less than 24 h when changing the power generated. An oversampling and averaging technique was utilized in the temperature acquisition. There were 20 readings from each channel sampled at a rate of 80 Hz, averaged and stored. All channels were sampled every 30 min to determine if steady-state conditions existed. Steady-state conditions were assumed to occur when the average temperature for each location varied by less than 0.3°C. The steady-state temperatures reported consisted of the average of 20 readings taken from each channel. The maximum uncertainty in temperature was determined to be ±0.28°C (Ref. 6).

Numerical Model

A model of the ALR8(SI) storage assembly was created by the modification of an existing Pro/E solid model of the storage container shown in Fig. 1. The first step of the modification was removing one-half of the assembly due to symmetry. This reduced significantly the meshing and the solution efforts. Furthermore, the geometry was simplified at some locations and minor and irrelevant details such as bolt heads, nuts, rounding, and small gaps were eliminated.[6]

The solid components of the ALR8(SI) container were meshed with tetrahedral elements and corresponding material properties were assigned. The fluid volume shown represents the volume of the interior of ALR8(SI) that was filled with the corresponding backfill gas. This volume was also meshed with solid tetrahedral elements and was assigned material properties of the gas. Surfaces on which boundary conditions, symmetry, or thermal couplings were imposed were meshed with thin shell elements. SDRC I-DEAS Master Series 6 was used for both meshing and finite element analyses in this work. Separate finite element (FE) models were created from all of the components of the ALR8(SI) container, including the fluid volume. These FE models were then merged, forming one FE model of the ALR8(SI) container.

The FE model of the ALR8(SI) assembly had a finer mesh inside the container to allow higher accuracy in predicting the phenomena concerning gasdynamics and convection heat transfer. On the other hand, the sizes of the elements outside of the sealed insert, where pure heat conduction occurs, were larger. Approximately 20,000 total elements were used in this analysis, of which about 8000 were used in the fluid volume and 12,000 in the solid. Changing the number of elements in the fluid and solid volume by 50% changed the converged temperature distribution by less then 2%. Properties of the solid materials were kept constant for the simulations, whereas properties of the gases were corrected based on the mean temperature of the gas obtained by earlier simulations; thus, we effectively iterated to obtain the (constant) gas properties used for each simulation.

Boundary Conditions

Boundary conditions were imposed on the exterior surfaces of the Celotex, on the interior hemispherical surface of the plutonium pit, and on the surfaces that belonged to the symmetry plane. Because boundary conditions can be applied only on a surface mesh, these surfaces were meshed with triangular thin shell elements.

1) A heat load boundary condition was applied on the interior hemispheric surface of the pit simulator. The heat load was applied to thin shell elements with zero thickness.

2) A constant temperature boundary condition was applied to zero-thickness shell elements that enveloped the exterior of the Celotex.

3) A fluid flow symmetry plane boundary condition was applied to thin shell elements of the fluid volume that belonged to the symmetry plane.

4) An adiabatic symmetry boundary condition was applied to the remaining shell elements in the symmetry plane. These elements belonged to the solid components; their thickness was a small value greater than zero, and their thermal conductivity was zero. Hence, these elements were actively involved in the heat transfer calculations, but they prevented any heat transfer across this boundary and, thus, created an adiabatic wall condition.

When the FE models of the ALR8(SI) components were merged together into an assembled FE model, there existed no thermal connections between surfaces belonging to different components, although they were in contact. To create heat flowpaths between these components, thermal couplings were used. By effectively prescribing a thermal coupling type and numerical value, the heat flux passing from one surface to another was modeled. If the surfaces were in contact, the thermal coupling should actually model the contact resistance between the surfaces, if any. Furthermore, thermal couplings were applied between surfaces that were not in direct contact. In this case, the thermal coupling modeled the thermal resistance of the media between the surfaces.

Surfaces that were to be coupled were coated with thin shell, zero-thickness elements. A group of elements was made from the elements of each surface. These groups were chosen when defining a specific type of thermal coupling, and a numerical value was assigned to each group. The thermal coupling works such that, for every element of the primary group, a corresponding (closest) secondary element was found, and a heat transfer path was created characterized by the type and the value of the coupling.

Heat Transfer Coefficient Thermal Couplings

The heat transfer from the primary to the secondary elements, in this case, was modeled by specifying a numerical value of a heat transfer coefficient. This coefficient in a general case was derived from the following equation, in watts per square meter Kelvin:

$$h = k/\delta \tag{6}$$

Generally, if a thermal contact resistance of a specific interface was known, the heat transfer coefficient was calculated as $h = 1/R$, where R is the thermal contact resistance found in the literature. If the gap between the surfaces was filled with a solid medium, it was easy to find the heat transfer coefficient using Eq. (6). However, it was more complex to define the coefficient if a gaseous medium filled the small gap between the surfaces, which happened in most of the cases in this problem. In this case, the heat transfer coefficient was approximated from the following equation:

$$h = kC_aC_r/\delta = (k/\delta)C \tag{7}$$

In Eq. (7), C_a and C_r are coefficients that take into consideration the heat advection in the gaseous medium and the radiation exchange between the surfaces separated by the gaseous medium, respectively. Because it was very difficult to predict these coefficients precisely, they can be multiplied together into one coefficient ($C = C_aC_r$). In this form, the coefficient C actually indicates how much more heat can be transferred across the gap as compared to the heat transfer occurring by pure conduction through the gaseous medium.

The coefficient C depended on the temperature difference expected between the surfaces separated by the gap, the geometry of the gap, and other factors. The geometry of the gap, in the global view of the heat transfer occurring in the ALR8(SI), provided an idea as to what extent favorable conditions for convection or radiation existed. Consequently, modeling a thermal coupling between surfaces separated by a gas gap was reduced to approximating the coefficient C. However, defining the coefficient C for the variety of contact surfaces and gaps existing in the ALR8(SI) was a very complicated task and could not be determined analytically. Therefore, experimental data served as an empirical ground for approximating the coefficient C, and ultimately the thermal resistances. In Table 1, ranges of the thermal resistance used for all existing thermal couplings in all of the various simulations are given. Obtaining the values listed in Table 1 required that the initial estimates of C, based purely on C_a, be adjusted to account for radiation, so that the simulated temperature distribution for one experimental case approached the actual experimental distribution. Once values of the coefficients were determined, for which the simulation closely matched the experimental temperatures, the same values were used for all experimental cases with the same thermal generation rate. Higher heat generation rates resulted in higher values of the coefficient C because higher heat generation rates increased the temperature difference between adjacent surfaces separated by a gap and, hence, radiation effects increased. Locations of the thermal contacts (gaps) that required the coefficient C are presented in Fig. 3.

Radiation was modeled within the three enclosures that correspond to the three subvolumes formed by the birdcage disks and the walls of the sealed insert. A group of thin shell elements with prescribed emissivity was created from each surface within each subvolume. An emissivity of 0.2 was used for stainless steel. Radiation thermal couplings were defined between groups, that is, between each pair of surfaces in the corresponding enclosure. These surfaces radiated heat from the hotter elements to the colder ones according to the following equation:

$$q = \sigma F_{ij} A\left(T_{\text{hot}}^2 + T_{\text{cold}}^2\right)(T_{\text{hot}} + T_{\text{cold}})(T_{\text{hot}} - T_{\text{cold}}) \tag{8}$$

For every radiation thermal coupling, a view factor was calculated based on the geometry of the corresponding surfaces.

Table 1 Thermal resistance of the contacts/gaps as illustrated in Fig. 3

Thermal coupling	Thermal resistance, m^2K/W
1	0.063–0.031
2A	0.0033–0.001
2B	0.033–0.01
3	0.0001
4	0.0068–0.002
5A	0.0033–0.001
5B	0.0125–0.004
5C	0.0083–0.0025
6	0.0083–0.0025
7	0.05–0.0125
8	0.0068–0.002

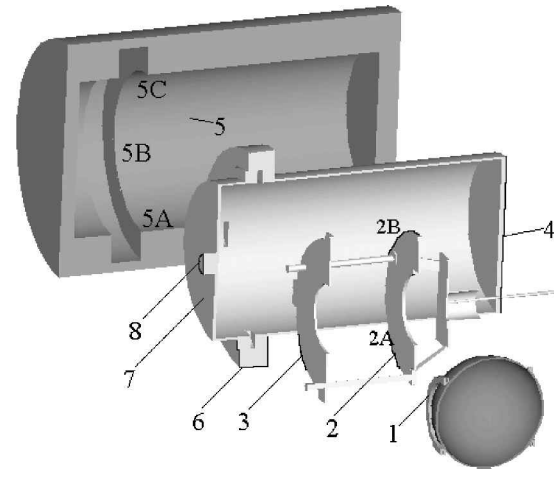

Fig. 3 Thermal contacts and gaps in the sealed insert.

Solution Procedure

The FE model was solved simultaneously by a thermal and a flow SDRC I-DEAS ESC solver by switching between the thermal domain and the fluid domain of the model. The thermal domain consisted of the solid components. A three-dimensional steady-state solution was obtained by solving the heat diffusion equation. On the other hand, the solution of the flow domain was iterated in time to its steady-state solution using a physical time step of 0.1 s because there was not a steady-state fluid solver. Every 10 iterations of the flow solver, both the steady-state thermal and unsteady flow domains solutions were coupled because they shared common temperatures at their interface. The final steady-state solution was obtained when the convergence parameters fell below a prescribed value, for the flow solution, when momentum, mass, and total energy residuals fell below 10^{-5}, and for the coupled solution, when the residual heat imbalance fell below 10^{-7}.

The I-DEAS ESC thermal analysis software uses a control volume approach in formulating the discrete finite difference (FD) equations that approximate the governing partial differential equations. This method, also known as the lumped parameter method, is based on conservation of energy applied both locally and globally within the domain. This technique involves the geometrical discretization or meshing of the model into control volume regions and establishing, within each region, a calculation point called the FD calculation point. Heat balance equations are established for each of these control volumes.

The flow solver computes a solution to the nonlinear, coupled, partial differential equations for the conservation of mass, energy, and momentum in general complex three-dimensional geometry. It uses an element-based finite volume method and a coupled algebraic multigrid method to discretize and solve the governing equations. For the analysis of the ALR8(SI), the laminar flow model was used with the Boussinesq approximation[4] for buoyancy.

Results and Discussion

The thermal response of the ALR8(SI) under normal storage conditions was investigated as a function of heat generation rate (15, 20,

Table 2 Comparison of experimental and numerical temperatures (°C) for locations 1–6 and 8–10 as illustrated in Fig. 2

	20°C 15 W		20°C 20 W		25°C 15 W		25°C 20 W	
Location	Experimental	Numerical	Experimental	Numerical	Experimental	Numerical	Experimental	Numerical
				Air				
1	47.7	46.5	55.5	53.8	52.4	51.5	58.8	58.8
2	46.6	46.0	52.8	53.4	50.0	51.3	56.6	58.4
3	46.7	46.5	53.3	54.0	50.4	51.6	57.2	59.2
4	49.6	47.2	56.9	55.0	53.0	52.2	60.6	60.0
5	52.9	49.4	59.0	56.4	55.1	53.4	63.1	61.4
6	38.7	37.3	43.1	42.9	42.3	42.5	46.9	48.1
8	34.4	35.1	37.8	40.2	38.3	40.4	41.7	45.0
9	41.8	39.0	47.0	45.0	45.3	43.9	50.7	50.2
10	36.2	36.0	39.9	41.1	39.7	40.8	43.5	46.2
				Argon				
1	51.6	50.5	58.8	58.3	54.6	55.4	61.7	63.1
2	49.6	50.0	55.6	57.7	53.0	55.0	59.0	62.5
3	50.2	50.6	56.5	58.5	53.9	55.6	60.2	63.5
4	53.0	51.2	60.0	59.6	56.5	56.1	63.5	64.4
5	54.3	52.2	60.8	61.1	58.4	57.1	65.1	65.7
6	40.0	38.2	43.7	44.0	43.7	43.0	47.3	49.0
8	36.2	36.0	38.4	41.5	39.5	40.8	42.6	46.0
9	43.8	40.2	48.5	47.0	47.4	45.1	51.9	52.0
10	38.4	37.0	41.6	43.0	41.8	42.0	45.0	47.5
				Helium				
1	42.8	41.3	48.0	47.0	46.7	44.3	52.1	50.0
2	42.0	41.6	47.4	47.5	45.3	44.7	50.2	50.5
3	41.5	41.8	46.8	47.9	44.8	44.8	49.9	50.8
4	43.6	41.5	49.2	47.5	46.7	44.4	52.3	50.4
5	47.0	43.3	53.6	49.8	49.1	46.2	55.9	52.8
6	37.6	36.7	41.7	42.0	41.2	41.6	45.0	46.8
8	33.3	34.7	36.1	39.4	37.6	39.6	40.1	44.4
9	38.9	37.3	43.4	42.5	42.3	42.2	46.5	47.6
10	34.4	34.7	37.5	39.4	38.0	39.6	40.8	44.4

25, and 30 W), outside container temperature (20, 25, and 30°C), and backfill gas (air, argon, and helium).

A comparison between the temperatures obtained numerically and experimentally for nine locations on the pit simulator and the birdcage are presented in Table 2. The pit simulator and the birdcage experience the highest temperatures, and their temperature distribution varies in a more obvious manner as a function of the boundary and heat generation conditions as compared to the other components within the ALR8(SI) container. Examining the data in Table 2 reveals a maximum discrepancy of 4°C between the numerical and the experimental temperatures. In general, the average temperature difference is approximately 2°C. A comparison between the numerical and the experimental average temperature of the pit simulator calculated from the five experimental locations on the pit's surface for the 25°C boundary temperature is plotted in Fig. 4 as a function the heat generation rate for each of the different backfill gases.

A vivid inspection into the numerically obtained temperature distribution of ALR8(SI) components, as well as the temperature of the backfill gas, for the experimental case of 15-W heat generation and 25°C boundary temperature with helium as the backfill gas is illustrated in Figs. 5–7. Figure 5 shows the temperature distribution of the steel components (the sealed insert, the birdcage, and the pit simulator). It can be seen that the pit contains the highest temperatures, and a large temperature difference exists between the pit and the birdcage. This indicates a poor heat conduction path from the pit to the birdcage that is caused by a neoprene gasket that separates the pit from the birdcage. The temperature distribution of the solid components in the symmetry plane is shown in Fig. 6 and illustrates that Celotex, although used as a packing material, serves effectively as an insulator, irrespective of the backfill gas. These two temperature drops, namely, the one between the pit simulator and the birdcage, and the other across the Celotex, are the main reasons for the relatively high temperatures of the ALR8(SI) interior.

The temperature of the helium in the symmetry plane is shown in Fig. 7, where the difference between the hottest and coldest portions of the helium is 12°C. (Note that the same difference using argon as the backfill gas is 20°C.) The helium velocity distribution at the symmetry plane, as given in Fig. 8, indicates a low-magnitude circular movement within each subvolume formed due to the birdcage (Fig. 3). The birdcage restricts the flow of gas between the three subvolumes that it creates. The maximum velocity occurs in the smallest and largest subvolumes and is about twice that found in the middle subvolume. This velocity trend in the respective subvolumes also occurred when either argon or air was the backfill gas. The argon velocity distribution on the symmetry plane for the same thermal conditions (15 W and 25°C) used in generating the data for Figs. 5–7 is presented in Fig. 9. The maximum velocity is approximately 100% greater when argon is the backfill gas as compared to helium, although the circulation patterns are similar.

From the backfill gases that have been considered in the experiments, the lowest temperatures of the sealed insert interior were achieved when it was filled with helium. A comparison of the maximum temperatures measured at position 5 (on the top of the pit simulator), for different backfill gases in the sealed insert is given in Fig. 10 for the 20 and 25°C boundary temperatures as a function of heat generation. As illustrated in Fig. 10, for a heat generation of 15 W, the maximum pit temperature was 7°C greater when argon was used as the backfill gas as compared to using helium and was 14°C greater for the 30-W heat generation rate case for the same two gases. Maximum pit temperatures using air as the backfill gas consistently fell between argon and helium. The experimental results showed that under steady-state conditions, the thermal requirement for the maximum temperature within the ALR8(SI) not to exceed 60°C was realized when helium was used as a backfill gas for heat generation rates of 20 W and isothermal boundary temperatures less than 25°C.

The numerical analysis provided a means to determine which heat transfer mechanism(s) caused the significant difference in maximum internal temperature that were realized both experimentally and computationally for the different backfill gases. The conduction paths through the solid birdcage structure, as well as the view factors between the pit and the sealed insert, remain unchanged as the

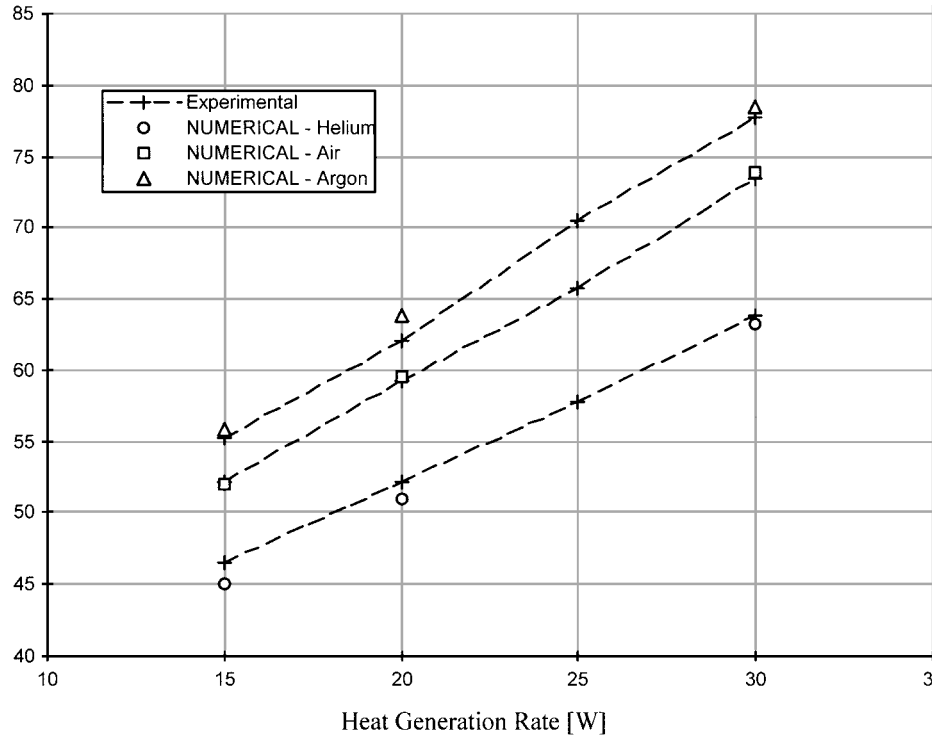

Fig. 4 Comparison of numerical and experimental average pit temperatures for the 25°C boundary temperature; – – –, added to the experimental data for clarity.

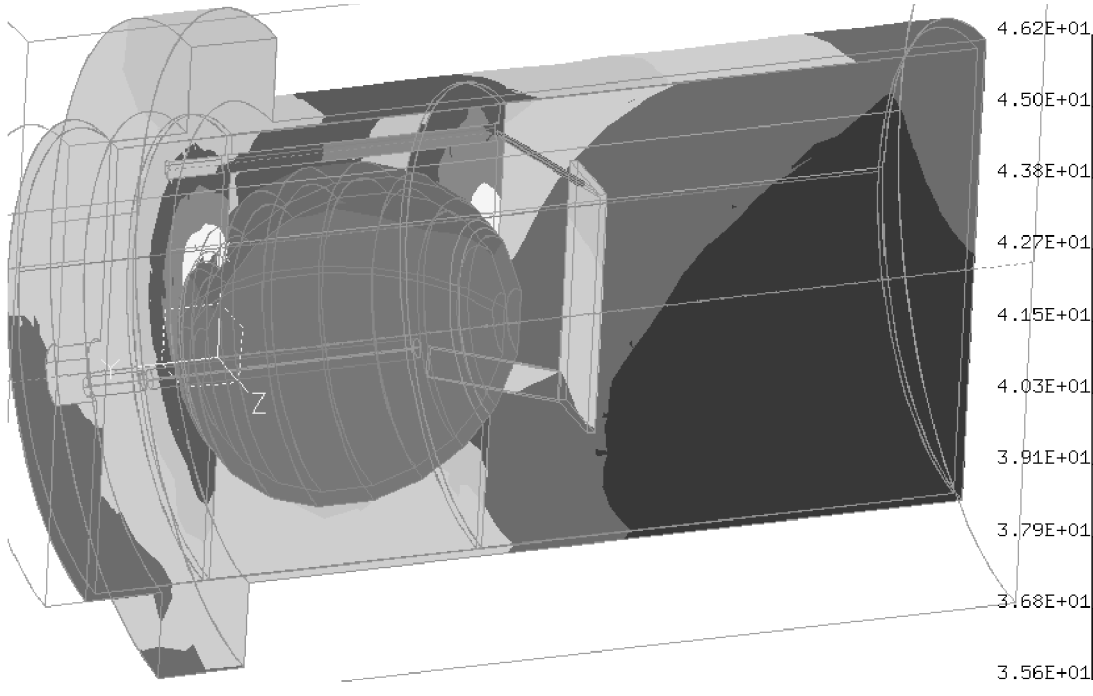

Fig. 5 Temperature distribution of the steel components: 15 W, 25°C, helium.

backfill gas is changed. Conduction heat transfer through the birdcage is hampered by the neoprene ring that is affixed to the birdcage in areas that contact the pit and the many contact resistances between the pit and the inner surface of the sealed insert. The small temperature differences that existed between the pit surface and the inner surface of the sealed insert for each backfill gas were not sufficient for radiation to be the cause for the difference in maximum internal temperature. Neither conduction through the birdcage nor radiation in a nonparticipating media would be dependent on the backfill gas. Natural convection, however, would be dependent on the backfill gas because each gas has different thermal–physical properties. Thus, an investigation into natural convection heat transfer within an enclosure was performed to better understand what was occurring within the sealed insert and how the gas properties affected heat transfer.

An indicator as to the degree and type of natural convection is the gap-based Rayleigh number Ra_L, which is defined as

$$Ra_L = Gr_L Pr \tag{9}$$

where the Grashof number is defined as

$$Gr_L = g\beta \Delta T L^3/\nu^2 \tag{10}$$

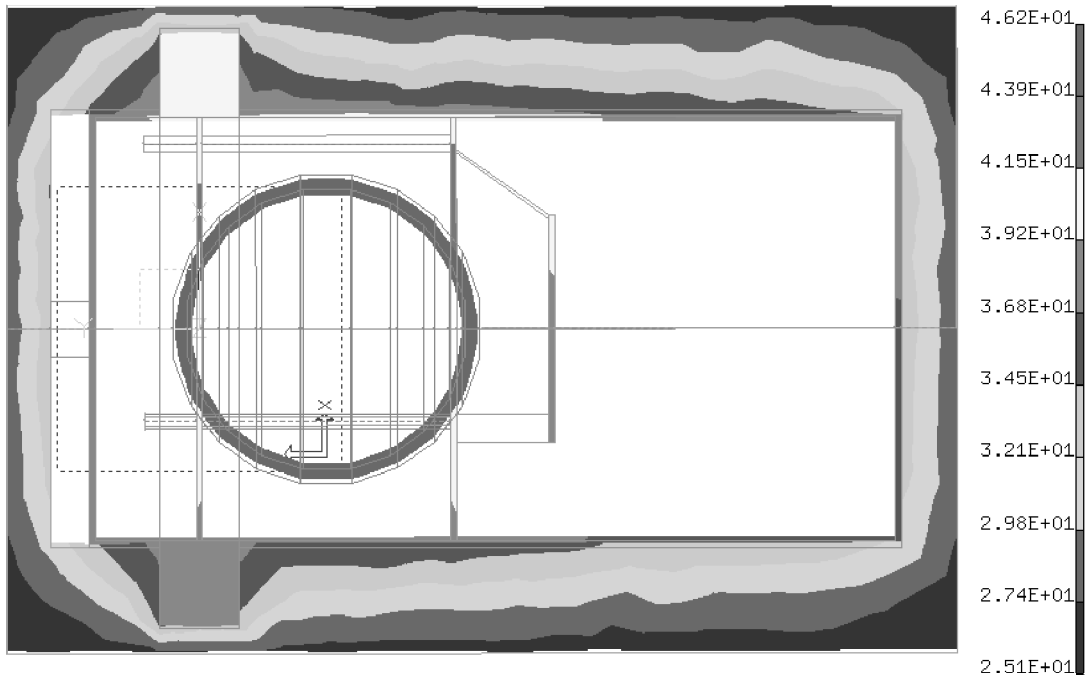

Fig. 6 Temperature distribution of the solid component on the symmetry plane: 15 W, 25°C, helium.

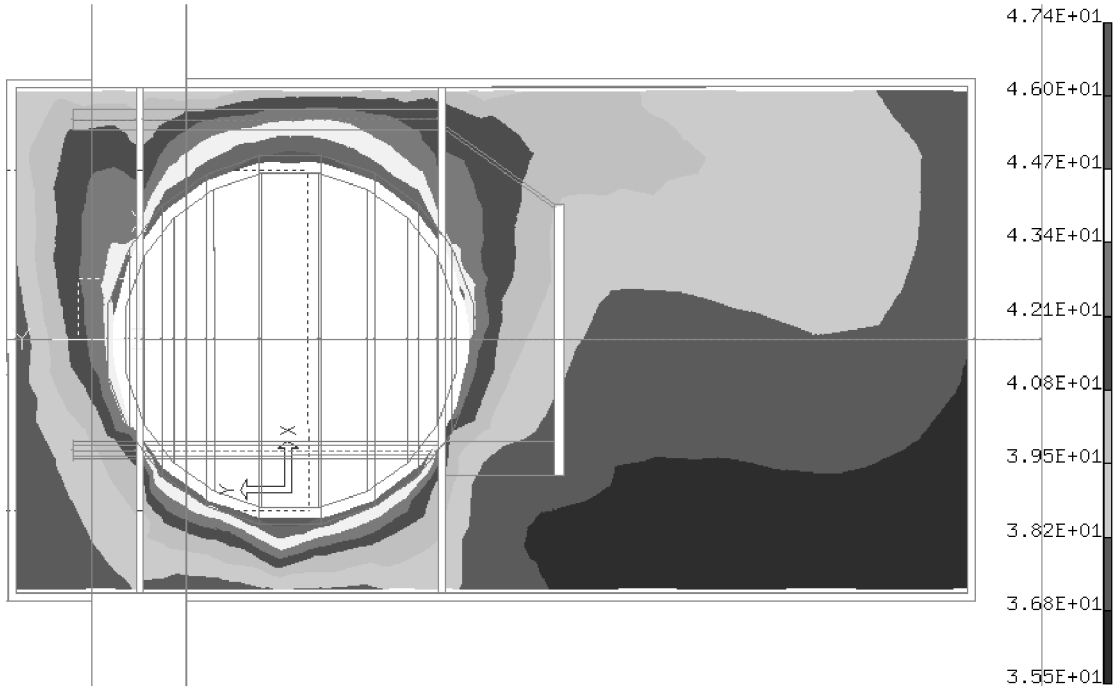

Fig. 7 Temperature of the helium gas, symmetry plane: 15 W, 25°C, helium.

Experimental work concerning natural convection in concentric cylinders[7–11] indicates that, as long as the gap-based Rayleigh number is less than 10^7, laminar natural convection exists. Evaluating the gap-based Rayleigh number for each of the three backfill gases based on the largest temperature difference within the middle subvolume of the sealed insert yields a Rayleigh number of slightly more than 10^5 for both air and argon and 10^3 for helium. Thus, laminar natural convection exists within the ALR8(SI) container.

The bulk of the simulated pit is contained within the middle subvolume, and as a first approximation, this region can be considered similar to the case of heat transfer within concentric cylinders. Natural convection heat transfer in the annular region between long, horizontal cylinders has been considered previously.[12] For this configuration, the pit simulator corresponds to the inner cylinder that is heated, and the sealed insert corresponds to the outer, cooled cylinder. The heat transfer rate per unit length may be expressed as[12]

$$q' = \frac{2\pi k_{\text{eff}}}{\ln(D_o/D_i)}(\Delta T) \tag{11}$$

where the suggested correlation of the effective thermal conductivity k_{eff} is

$$k_{\text{eff}} = 0.386\left(\frac{Pr}{0.861 + Pr}\right)^{\frac{1}{4}}\left(Ra_c^*\right)^{\frac{1}{4}}k \tag{12}$$

$$Ra_c^* = \frac{[\ln(D_o/D_i)]^4}{L^3\left(D_i^{-\frac{3}{5}} + D_o^{-\frac{3}{5}}\right)^5}Ra_L \tag{13}$$

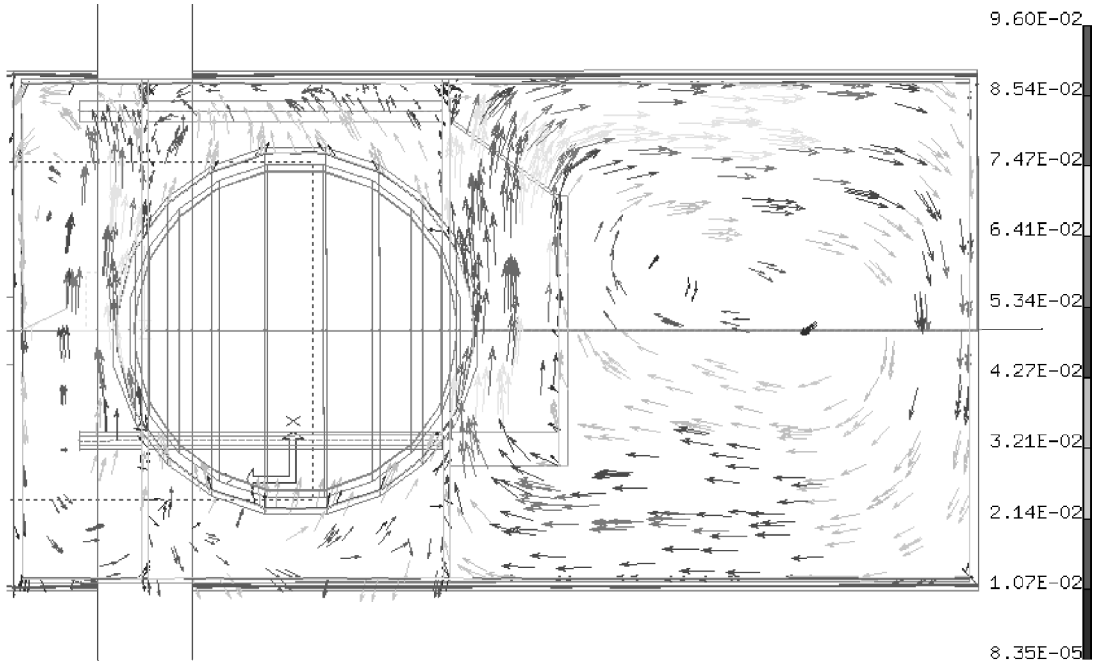

Fig. 8 Velocity of the helium gas, symmetry plane: 15 W, 25°C, helium.

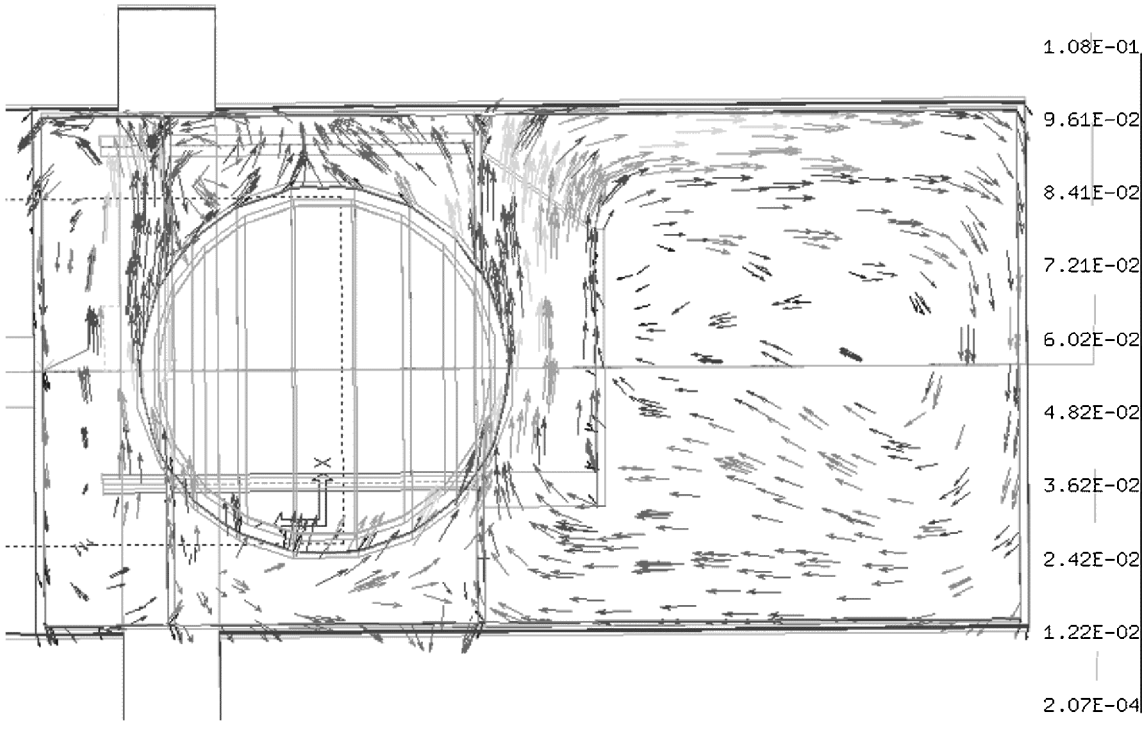

Fig. 9 Velocity of the argon gas, symmetry plane: 15 W, 25°C, argon.

The Rayleigh number Ra_L in Eq. (13) is evaluated using Eqs. (9) and (10). The temperature difference in Eq. (11) is that of the inner (pit wall) and outer surfaces (sealed insert). The following expression for the heat transfer rate is obtained by substituting Eqs. (12) and (13) into Eq. (11):

$$q' = 0.772\pi(g\beta)^{\frac{1}{4}}\left[\frac{T_i - T_o}{D_i^{-\frac{3}{5}} + D_o^{-\frac{3}{5}}}\right]^{\frac{5}{4}}\left[\frac{\sqrt{Pr}}{(0.861 + Pr)^{\frac{1}{4}}}\right]\left[\frac{k}{\sqrt{\nu}}\right] \tag{14}$$

When Eq. (14) is examined, the only parameters that vary significantly are the thermal conductivity and the kinematic viscosity. It is Eq. (11), however, that can be most easily used to identify which heat transfer mechanisms are dominant within the sealed insert. The effective conductivity k_{eff}, defined in Eq. (12), and the Rayleigh number that is contained in the definition of k_{eff} indicate whether conduction through the gas or natural convection are the primary means by which heat is transferred within the sealed insert.

Considering helium, Rayleigh number Ra_L was calculated to be approximately 10^3 and k_{eff}/k was less than one. It is noted in Ref. 13 that for an enclosure heated from below, the critical Rayleigh number for which natural convection becomes important relative to conduction through the fluid is 1708, and in Ref. 12 that a ratio of k_{eff}/k less than one implies that there is no enhancement of heat transfer caused

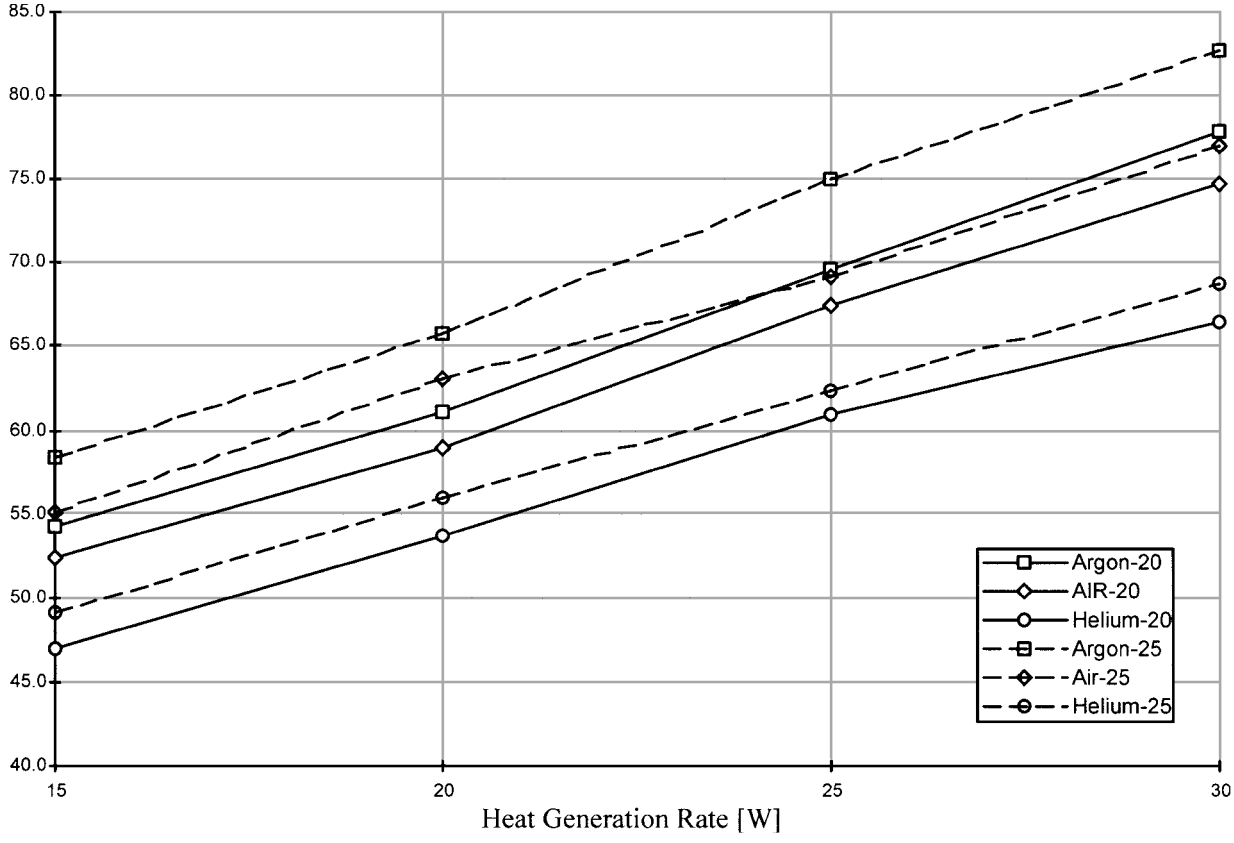

Fig. 10 Maximum simulated pit temperature as a function of heat generation rate for the 20 and 25°C boundary temperature.

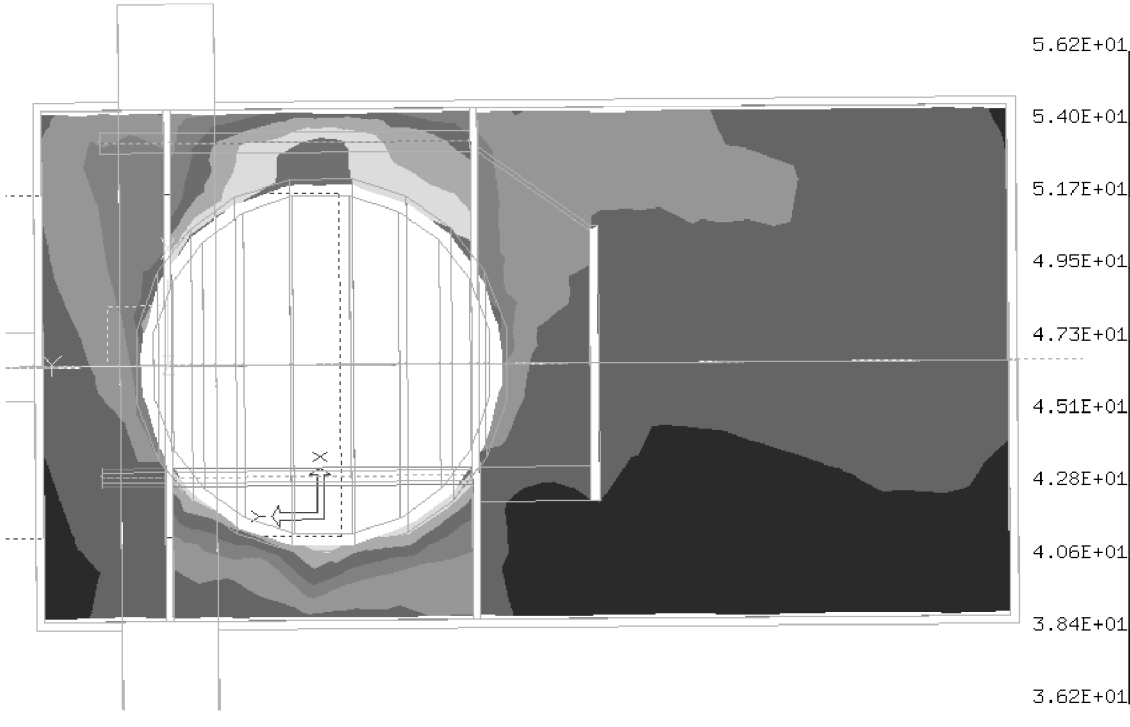

Fig. 11 Temperature of the argon gas, symmetry plane: 15 W, 25°C, argon.

by the motion of the fluid compared to pure conduction through the fluid.

For all cases tested, the ratio k_{eff}/k was less than one when helium was used as the backfill gas; therefore, the dominant heat transfer mechanism was conduction through the gas and not natural convection. This does not imply that the helium is stagnant within the container. In fact, the fluid does move, as was illustrated in Fig. 8, but not enough to convect heat to the wall of the sealed insert. Figure 7 depicts the temperature distribution in the middle subvolume, and it clearly shows that the temperature gradients are nearly radial, with no plume emanating from the top of the pit; thus, conduction through the gas is the primary heat transfer mechanism when helium is the backfill gas.

When argon, or air, on the other hand, is the backfill gas, Rayleigh number Ra_L was calculated on the order of 10^5 and k_{eff}/k was greater than one, indicating that natural convection within the sealed

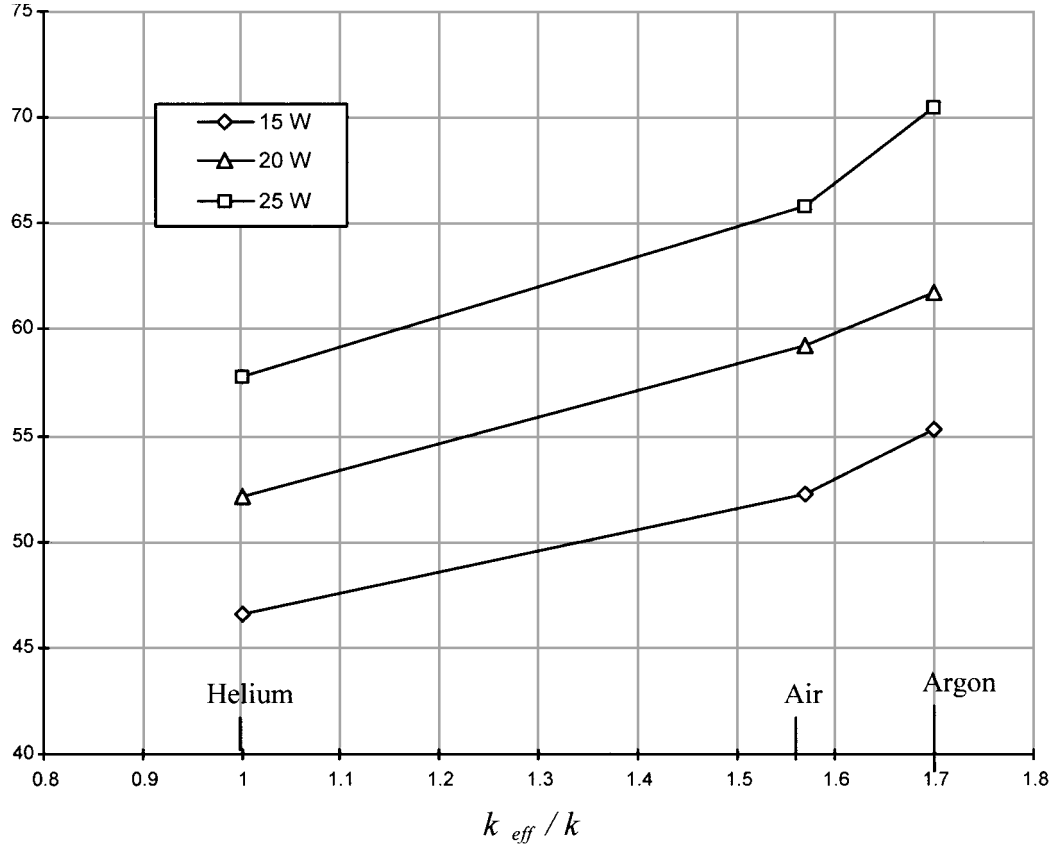

Fig. 12 Average temperature of the pit simulator for the 25° C boundary temperature as a function of the effective conductivity.

insert was the dominant mode of heat transfer. The temperature distribution for argon is given in Fig. 11, and it clearly shows a plume at the top of the simulated pit, indicating that natural convection is occurring. Similar temperature profiles occurred when air was the backfill gas.

The average temperature of the five locations on the pit simulator surface is plotted as a function of k_{eff}/k in Fig. 12 for the different backfill gases and the 25°C boundary temperature. Figure 12 clearly shows that the average pit temperature in the interior of the ALR8(SI) container depends on the properties of the gas used to fill the sealed insert. Thus, as a predictive tool to determine if a different backfill gas would keep the ALR8(SI) interior cooler than when helium is the backfill gas, one must calculate the effective conductivity (use the molecular thermal conductivity if the effective conductivity is less than one) and compare that value with the molecular thermal conductivity of helium for the same boundary conditions. The backfill gas with the greater conductivity will result in a cooler ALR8(SI) interior.

The insight gained by the simplified heat transfer analysis was used to make changes within the sealed insert for the purpose of increasing heat transfer away from the pit. The predicted velocity distributions indicated that connecting the three subvolumes would enhance heat transfer, such that circulation of the backfill gas would occur across the whole volume of the sealed insert. The ALR8(SI) numerical model was changed by creating slots in the discs of the birdcage, as presented in Fig. 13. The slots spanned most of the width of the birdcage, had an included angle of 60 deg (30 deg when considering symmetry), and were located at the top and bottom of the birdcage. Figure 14 shows the temperature distribution of the steel components for the modified birdcage using helium as the backfill gas. When these results are compared with temperatures of the ALR8(SI) steel components for the standard birdcage (Fig. 5), it can be seen that the maximum temperature is reduced by 8°C. When argon is used as the backfill gas, the maximum temperature is reduced by only 3.5°C. The modification of the birdcage is more

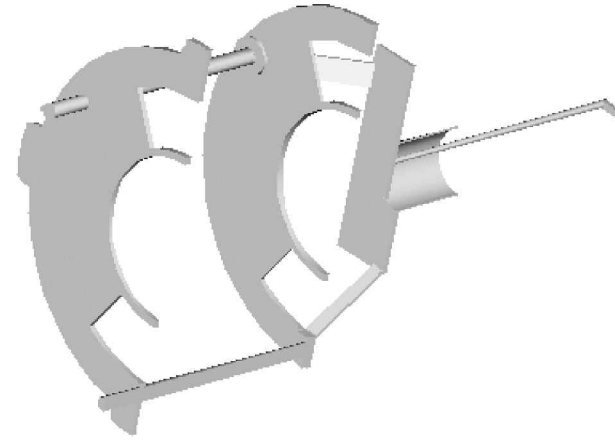

Fig. 13 Modified birdcage with slots.

effective when helium is the backfill gas as compared with argon because the axial movement of the helium through the openings made in the birdcage, as illustrated in Fig. 15, provides a more uniform gas temperature distribution in the three subvolumes and, consequently, lower temperatures of the ALR8(SI) interior.

The numerical analysis further suggested that in addition to the changes in the birdcage, orienting the container at an angle, thus providing a portion of the gravity vector along the axis of the container, would enhance the circulation of the gas throughout the entire sealed insert volume by increasing the natural convection heat transfer. This would be especially beneficial when helium is the backfill gas because the gap-based Rayleigh number for the largest subvolume increases significantly (by more than a factor of 50) as the container storage position is changed from horizontal (the stage-right configuration) to vertical with the pit near the floor.

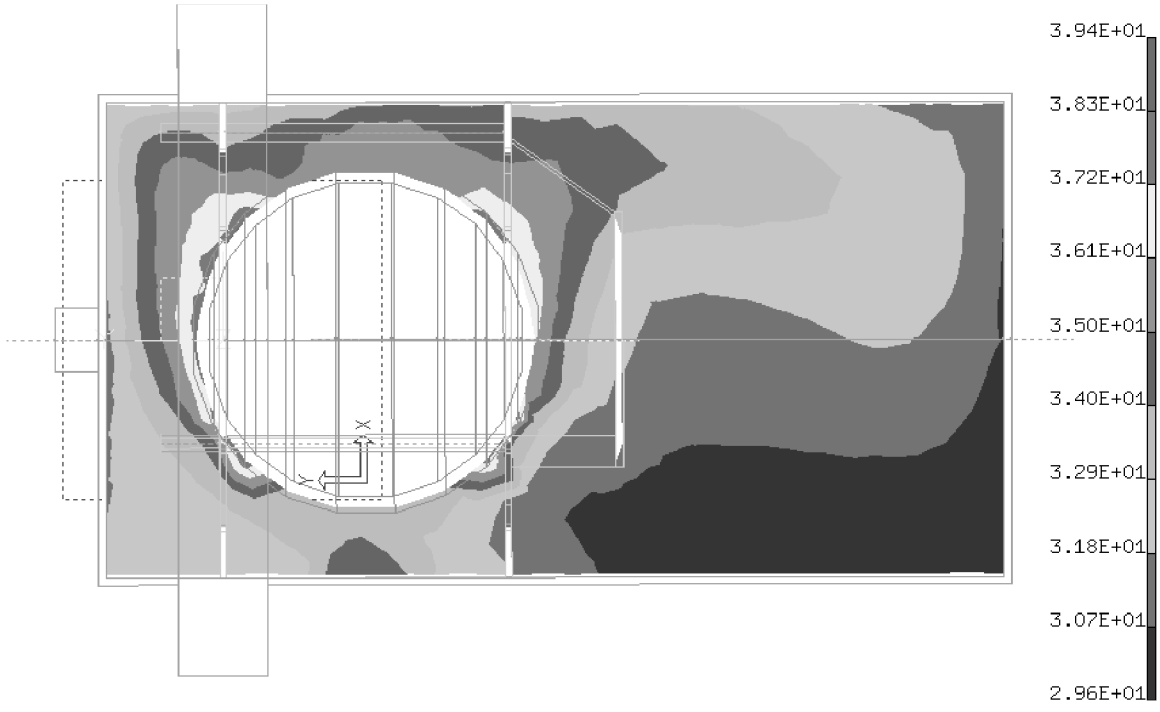

Fig. 14 Temperature distribution of the helium gas on the symmetry plane with the modified birdcage: 15 W, 25°C, helium.

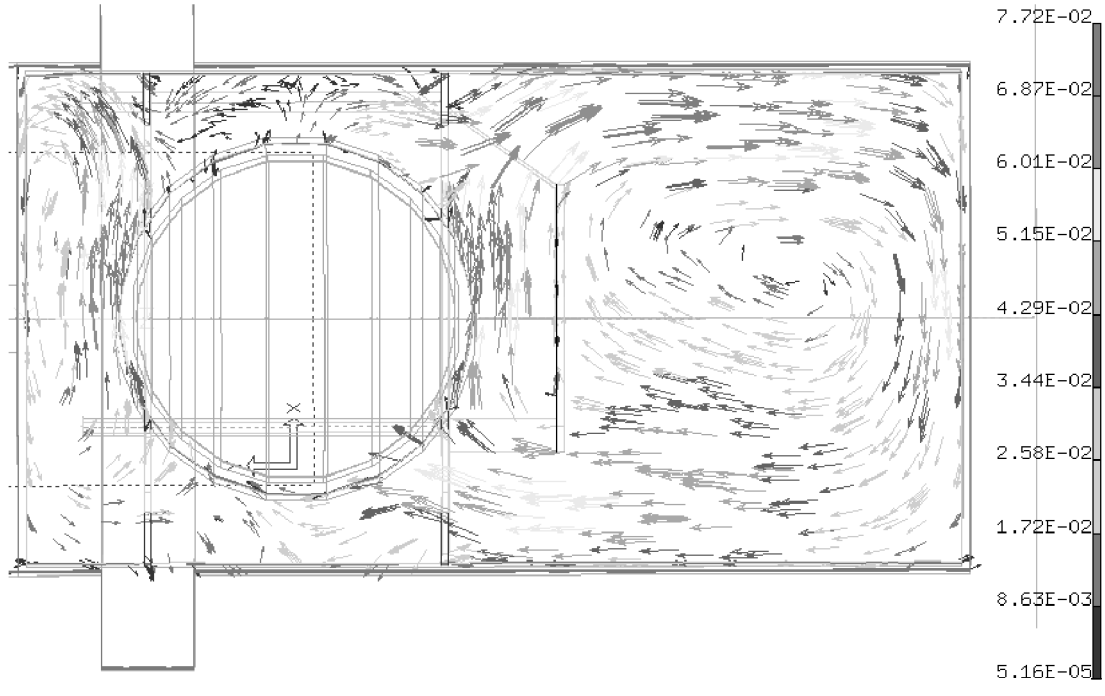

Fig. 15 Velocity distribution of the helium gas on the symmetry plane with the modified birdcage: 15 W, 25°C, helium.

Conclusions

The results of this work showed that, under steady-state conditions, the thermal requirement for the maximum temperature within the ALR8(SI) not to exceed 60°C was realized when helium was used as a backfill gas for heat generation rates up to 20 W and isothermal boundary temperatures less than 25°C.

By the use of a simplified natural convection analysis of heat transfer in the middle subvolume, conduction through the gas was identified as the primary mode of heat transfer within the sealed insert when the backfill gas was helium. Natural convection was the primary mode of heat transfer within the sealed insert when argon or air was the backfill gas. In fact, calculations based on the simulated temperature distribution show that less than 0.5 W of the 15 W of heat generated in the pit simulator was conducted from the pit through the birdcage, irrespective of the backfill gas. The reason that conduction heat transfer through the birdcage was so low was the neoprene gasket that "isolated" the pit from the birdcage housing. Radiative heat transfer for the 15-W heat generation was approximately 3.5 and 1.4 W when argon and helium were used as the backfill gas, respectively.

Predicted temperatures from numerical heat transfer simulations matched the experimental data well and generally differed by less than 2°C. The birdcage was modified by cutting slots into it using the numerical model. Simulations of the modified birdcage predicted

lower pit temperatures for all three backfill gases. The numerical data showed that the slots provided axial flow between the subvolumes that were formed by the birdcage, resulting in enhanced heat transfer to the surroundings. The decrease in pit temperatures was greatest when helium was the backfill gas. Further reductions in the pit temperature could be realized by orienting the ALR8(SI) container at an angle, such that the longitudinal axis of the container and gravity were more aligned, if not parallel. This orientation would significantly enhance natural convection heat transfer because the backfill gas would circulate through the entire interior of the sealed insert.

Acknowledgments

This work was prepared with the support of the U.S. Department of Energy, Cooperative Agreement DE-FC04-95AL85832, and was conducted through the Amarillo National Resource Center (ANRC). The authors thank the ANRC and Mason & Hanger Corp. for their support of this work.

References

[1]Hensel, S. J., Lee, S. Y., and Schaade, J. B., "Plutonium Storage Thermal Analysis," *Transportation, Storage, and Disposal of Radioactive Material*, PVP-ASME, American Society of Mechanical Engineers, Fairfield, NJ, Vol. 348, 1997, pp. 57–65.

[2]Feldman, M. R., and Anderson, J. C., "Thermal Analysis of the Horizontal Shipping Container for Normal Conditions of Transport with Solar Insolation," Rept. Y/LF-456/R1, Oak Ridge Y-12 Plant, Oak Ridge, TN, April 1993.

[3]Öziçik, N. M., *Heat Conduction*, Wiley, New York, 1993, p. 11.

[4]Incropera, F. P., and DeWitt, D. P., *Fundamentals of Heat and Mass Transfer*, Wiley, New York, 1996, pp. 485–487.

[5]"SDRC I-DEAS Master Series 6," CAE Software, Structural Dynamics Research Corp., Dallas, TX, 1998.

[6]Stevkovski, S., "Thermal Analysis of Plutonium Storage Containers," M.S. Thesis, Mechanical Engineering Dept., Texas Tech Univ., Lubbock, TX, Aug. 1999.

[7]Bishop, E. H., "Heat Transfer by Natural Convection of Helium Between Horizontal Isothermal Concentric Cylinders at Cryogenic Temperature," *Journal of Heat Transfer*, Vol. 110, No. 1, 1988, pp. 109–115.

[8]Grigull, U., and Hauf, W., "Natural Convection in Horizontal Cylindrical Annuli," *Third International Heat Transfer Conference*, Vol. 2, Science Press, Ephrata, PA, 1966, pp. 182–195.

[9]Lis, J., "Experimental Investigation of Natural Convection Heat Transfer in Simple and Obstructed Horizontal Annuli," *Third International Heat Transfer Conference*, Vol. 2, Science Press, Ephrata, PA, 1966, pp. 196–204.

[10]Liu, C., Mueller, W. K., and Landis, F., "Natural Convection Heat Transfer in Long Horizontal Cylindrical Annuli," *International Developments in Heat Transfer*, American Society of Mechanical Engineers, New York, 1963, pp. 976–984.

[11]Kuehn, T. H., and Goldstein, R. J., "An Experimental Study of Natural Convection Heat Transfer in Concentric and Eccentric Horizontal Cylindrical Annuli," *Journal of Heat Transfer*, Vol. 100, No. 2, 1978, pp. 635–640.

[12]Raithby, G. D., and Hollands, K. G. T., "A General Method of Obtaining Approximate Solutions to Laminar and Turbulent Free Convection Problems," *Advances in Heat Transfer*, Vol. 11, Academic Press, New York, 1975, pp. 265–315.

[13]Bejan, A., *Convection Heat Transfer*, 2nd ed., Wiley, New York, 1996, pp. 252–254.